Intrinsic Fluorescence Reports a Global Conformational Change in the N-Lobe of Human Serum Transferrin following Iron Release†

Nicholas G. James,‡ Christopher L. Berger,§ Shaina L. Byrne,‡ Valerie C. Smith,|| Ross T. A. MacGillivray,|| and Anne B. Mason*,‡

Department of Biochemistry, 89 Beaumont Avenue, and Department of Molecular Physiology and Biophysics, 149 Beaumont Avenue, College of Medicine, University of Vermont, Burlington, Vermont 05405, and Department of Biochemistry and Molecular Biology, University of British Columbia, Vancouver, British Columbia V6T 1Z3, Canada

Received November 22, 2006; Revised Manuscript Received July 6, 2007

ABSTRACT: Transferrins have been extensively studied in order to understand how they reversibly bind and release iron. Human serum transferrin (hTF) is a single polypeptide chain that folds into two lobes (N- and C-lobe); each lobe binds a single ferric ion. Iron release induces a large conformational change in each lobe. At the putative endosomal pH of 5.6, measurement of the increase in intrinsic fluorescence upon iron release from the recombinant N-lobe yields two rate constants: 8.9 min^{-1} and 1.3 min^{-1}. Direct monitoring of iron release from the N-lobe at pH 5.6 (by the decrease in absorbance at 470 nm) gives a single rate constant of 9.1 min^{-1}, definitively establishing that the faster rate constant in the fluorescent studies is due to iron release. To further elucidate the molecular basis of the intrinsic fluorescence change (and the source of the slower rate constant), we examined the contributions of the three individual tryptophan residues in the N-lobe (Trp8, Trp128, and Trp264). Three double mutants, each containing the single remaining tryptophan residue, were produced. In the iron-bound N-lobe, Trp128 and Trp264 are quenched by iron and account for almost the entire fluorescent signal when iron is released. As for the wild-type N-lobe, the fluorescence increase for each of these mutants is best fit by a double-exponential function indicating two processes. Trp8 is severely quenched under all conditions, making virtually no contribution to the signal. Additionally, a mutant lacking all three Trp residues allows assignment of the fluorescent signal completely to the three tryptophan residues and observation of the presence of one (or more) tyrosinates in the N-lobe that have physiological significance in the uptake of iron.

Members of the transferrin (TF)[1] family are capable of sequestering ferric iron (Fe^{3+}), thus keeping it soluble and available for use in biologically important functions (i.e., oxygen transport, electron transport, etc.) (*1*, *2*). Human serum transferrin (hTF) plays a critical role in iron homeostasis by reversibly binding Fe^{3+} and transporting it to actively dividing cells via receptor-mediated endocytosis after binding to the specific transferrin receptor on the cell surface (*3*). Once iron-bound transferrin is inside the cell, the low pH (∼5.6) within the endosome facilitates iron release (*4*). Members of the TF family are each composed of a single polypeptide chain containing ∼700 amino acids (∼80 kDa) that folds to form two homologous lobes (N- and C-lobe) connected by a small linker peptide. The lobes can be further divided into subdomains (NI, NII, CI, and CII), each of which contributes ligands critical for Fe^{3+} binding. The subdomains form a cleft, in which a single Fe^{3+} is coordinated by an aspartic acid residue, two tyrosine residues, a histidine residue, and two oxygen atoms from the synergistic carbonate anion, anchored by an arginine residue (*5*). The Fe^{3+}-coordinating ligands are identical in almost all members of the TF family (*6*). X-ray crystallographic studies of hTF and of the N-lobe, with or without iron, provide snapshots of the large structural rearrangements between subdomains that occur in each lobe (*7*−*9*). A defining feature of the N-lobe is a pair of lysines that share a hydrogen bond in the iron form but are separated by 9 Å in the apo conformation (*10*, *11*).

In the case of the N-lobe, the two subdomains that form the cleft twist around a hinge at the bottom of the cleft to bind and release iron. The C-lobe has been less studied, although evidence clearly shows that the two lobes of hTF

† This work was supported by U.S. Public Health Service Grant R01 DK21739 (A.B.M.) and HL 63798 (C.L.B.) from the NIH.

* To whom correspondence should be addressed: phone (802) 656-0343; fax (802) 656-8220; e-mail anne.mason@uvm.edu.

‡ Department of Biochemistry, University of Vermont.

§ Department of Molecular Physiology and Biophysics, University of Vermont.

|| University of British Columbia.

[1] Abbreviations: WT, wild type; hTF, human serum transferrin; N-His hTF NG, recombinant nonglycosylated human serum transferrin with an N-terminal hexahistidine tag and a factor Xa cleavage site attached to the amino terminus of the protein; hTF N-lobe, recombinant N-lobe of human serum transferrin comprising residues 1−337; apo N-lobe, iron-free N-lobe; Fe N-lobe, iron-bound N-lobe; Trp128, double mutant W128Y/W264Y; Trp128, double mutant W8Y/W264; Trp264, double mutant W8Y/W128Y; null Trp mutant, triple mutant W8Y/W8Y/W264Y; DMEM-F12, Dulbecco's modified Eagle's medium−Ham F12 nutrient mixture; BHK, baby hamster kidney cells; UG, Ultroser G; FBS, fetal bovine serum; HRP, horseradish peroxidase; Tiron, 4,5 dihydroxyl-1,3-benzenedisulfonate; EDTA, ethylenediaminetetraacetic acid; MES, morpholinoethanesulfonic acid; HEPES, 4-(2-hydroxyethyl)-1-piperazineethanesulfonic acid; NaN_3, sodium azide; DTNB, 5 5′dithiobis(2-nitrobenzoic acid); GdnHCl, guanidine hydrochloride.

10.1021/bi602425c CCC: $37.00 © 2007 American Chemical Society
Published on Web 08/21/2007

differ in both their kinetic and thermodynamic properties (*12*, *13*). Specifically, release of iron from the N-lobe is faster and occurs at a higher pH than iron release from the C-lobe. Additionally, simple anions such as chloride slow the rate of iron release from the N-lobe at high pH and accelerate it at low pH with a crossover ~ pH 6.1; in contrast, the rate of release is increased at all pH values between 7.4 and 5.6 for the C-lobe (*14*). Understanding the molecular basis for these fundamental differences and their impact on the physiology of iron delivery to cells are important questions. A number of models of iron release from the N-lobe have been suggested (reviewed in ref *2*). The cumulative results support a pH-dependent release of iron in which cleft opening is the rate-limiting step. The acidic environment within the endosome causes protonation of the synergistic anion (carbonate) as the first step. Our crystal structure of the iron-loaded N-lobe of hTF (*8*) supports this claim. Protonation of the lysine pair (206 and 296) plays a key role in iron release by loosening the cleft. Mutating either lysine drastically retards the rate of iron release (*2*, *11*). Protonation of the histidine ligand (His249) further weakens the interaction with the bound iron. Protonation of Asp63, the single ligand from the NI subdomain, releases the subdomain to open freely and presumably allows entry of a chelator to release the iron from the two tyrosine ligands (*15*−*17*).

Over the past several decades, both absorbance and fluorescence assays have been used to monitor what is assumed to be the release of Fe^{3+} (*18*−*24*). Absorbance assays presumably directly measure the release of Fe^{3+} either as a decrease in the visible absorbance maximum (attributed to the metal−tyrosine interaction) or as an increase in formation of an iron chelator complex (*2*). Fluorescence assays monitor the increase in the fluorescent signal from tryptophan residues, which are quenched by the coordination of Fe^{3+} through radiationless transfer of electronic excited-state energy, as first described by Lehrer almost 40 years ago (*22*). This energy is transferred to an absorption band that overlaps the tryptophan fluorescence and is created by the metal−tyrosine interaction; it provides an early example of a Förster resonance energy transfer (FRET) mechanism. The quenching of tryptophan fluorescence by Fe^{3+} is lost when it is removed from hTF by a competing chelator. The recovery of intrinsic fluorescence intensity thus has been attributed to Fe^{3+} release from wild-type (WT) hTF and various hTF mutants (*25*, *26*). It is well-known that tryptophan fluorescence is also very sensitive to its immediate environment and therefore can function as a useful probe for detecting changes in local structure (*27*, *28*). For example, in transitioning from the apo to the iron-bound state, a small red shift (3−4 nm) is observed in hTF, indicating a metal-induced structural change around one or more of its tryptophan residue(s) (*22*).

Analysis of the hTF sequence reveals a total of eight tryptophan residues, three of which are found in the N-lobe (Figure 1). To simplify the interpretation of spectral and kinetic data, our laboratory has expressed substantial amounts of the isolated N-lobe as a recombinant entity (*29*). Structurally the isolated N-lobe (both with and without iron) is virtually identical to the N-lobe in full-length TF (*7*−*9*). It thus provides a suitable model for assessing the binding and release of iron from this lobe.

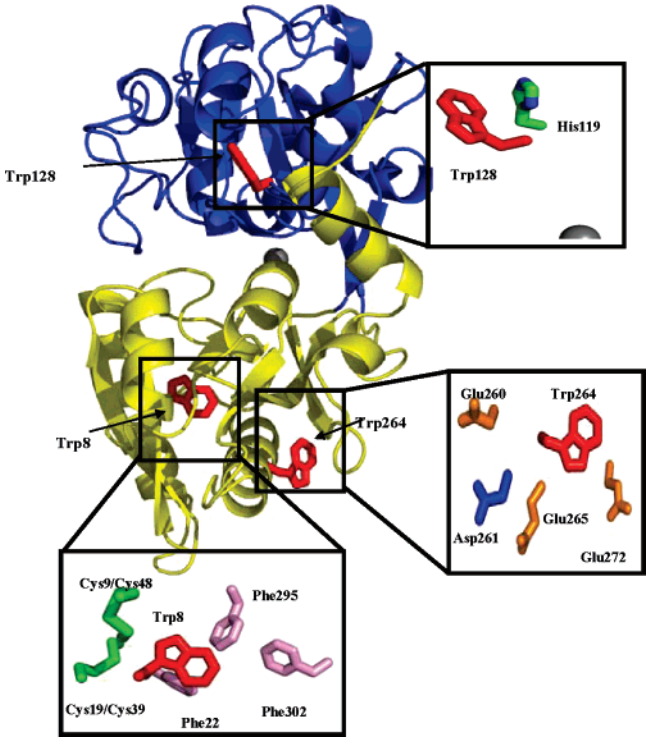

FIGURE 1: Crystal structure of WT Fe-hTF N-lobe (PDB 1A8E) showing the locations of the tryptophan residues Trp8, Trp128, and Trp264 (highlighted in red). The NI subdomain (yellow) and NII subdomain (blue) are indicated. The areas around each Trp residue have been enlarged to show nearby residues. Trp8 is ~27 Å from the iron center, Trp128 is at a distance of ~13 Å, and Trp264 is ~23 Å away.

In this work we clearly detect two rate constants for the increase in the fluorescent signal at pH 5.6. Absorbance measurements (A_{470nm}) at pH 5.6 show that the faster event is reporting iron release. In order to understand and to assign a molecular basis for the second slower rate constant, we examined the contributions of the three individual tryptophan residues in this lobe (Trp8, Trp128, and Trp264) to the fluorescent signal. Three double mutants, each containing the single remaining tryptophan residue, were produced and their spectral (absorbance and fluorescence) properties were determined. On the basis of this data, we suggest that the second rate constant is the result of conformational changes as reported by two of the three tryptophan residues in the N-lobe. No previous work on the N-lobe has provided rate constants specifically assigned to iron release and subsequent conformational change. Thus this work combines kinetic results with structural information to provide a more precise description of the steps leading to and immediately following iron release from the N-lobe of hTF.

MATERIALS AND METHODS

Materials. Dulbecco's modified Eagle's medium−Ham F-12 nutrient mixture (DMEM-F12), antibiotic−antimycotic solution (100×), trypsin, and acrylamide were from the Gibco−BRL Life Technologies Division of Invitrogen. Fetal bovine serum (FBS) was obtained from Atlanta Biologicals. Ultroser G (UG) is a serum replacement from Pall BioSepra (Cergy, France). The QuikChange mutagenesis kit and pBluescriptII were from Stratagene. Methotrexate was from Bedford Laboratories. Tiron was obtained from Fisher

Scientific. Poros 50 HQ resin was from Applied Biosystems. A Sephacryl S-200HR column was obtained from Amersham Pharmacia. EDTA was from the Mann Research Laboratories Inc. Ferrous ammonium sulfate and DTNB reagent were from Sigma. Centricon-10 microconcentrators, YM10 ultrafiltration membranes, and a spiral cartridge concentrator fitted with an S1Y10 cartridge were from Millipore/Amicon.

Preparation of Tryptophan N-Lobe Mutants. All mutants were introduced into the pNUT vector coding for the N-lobe (*29*) by use of the QuikChange site-directed mutagenesis kit. The mutagenic primers used to create single tryptophan point mutants have been reported previously (*24*). The three double tryptophan mutants were generated from the relevant single point mutants, and the triple mutant was generated from one of the double mutants. The WT hTF N-lobe and the double and triple point mutants were expressed by baby hamster kidney (BHK) cells containing the appropriate coding cDNAs in the pNUT vector and secreted into the tissue culture medium (DMEM−F12 10% FBS for batches 1−3 and DMEM-F12 1% UG + 1 mM butyric acid for batches 4−7), as previously reported (*30*). Purification of each mutant followed our standard protocol, which includes passage over an anion-exchange column (Poros 50 HQ) followed by separation of the N-lobe or the N-lobe mutants from bovine TF present in the media on a Sephacryl-200HR gel filtration column (*30*). SDS−PAGE was used to evaluate the homogeneity of the final product. Preparation of apo and iron-bound samples followed the procedures described previously (*11*).

Spectral Analysis. To assess the effect of amino acid substitutions on the visible spectrum, each iron-saturated mutant in 100 mM NH_4HCO_3 was scanned between 650 and 300 nm on a Varian Cary 100 spectrophotometer.

Determination of Molar Extinction Coefficient by the Edelhoch Method (31). Absorbance scans between 240 and 340 nm were collected for each protein in 100 mM NH_4HCO_3, pH ~8, and in 6 M guanidine hydrochloride (6 M GdnHCl). At the maximal absorbance in 6 M GdnHCl, ϵ at this wavelength is determined as follows:

$$\epsilon_\lambda = (\text{no. of Trp})\epsilon_{\lambda(\text{Trp})} + (\text{no. of Tyr})\epsilon_{\lambda(\text{Tyr})} + (\text{no. of Cys})\epsilon_{\lambda(\text{Cys})} \quad (1)$$

where the ϵ_λ values in 6 M GdnHCl for Trp, Tyr, and cystine are taken from Pace et al. (*32*). The protein concentration in 6 M GdnHCl is then calculated by use of the equation:

$$C(\text{6 M GdnHCl}) = A_\lambda(\text{6 M GdnHCl})/\epsilon_\lambda(\text{6 M GdnHCl}) \quad (2)$$

With this, the ϵ value at 280 nm of each protein in buffer is calculated from the relationship:

$$\epsilon_{280}(\text{buffer}) = A_{280}(\text{buffer})/C(\text{buffer}) \quad (3)$$

It is necessary to adjust the extinction coefficient of the apoprotein to account for the presence of Fe^{3+}. To achieve this, the A_{280} of each iron-containing protein in 100 mM HEPES buffer, pH 7.4, was obtained. An identical amount of protein was placed into 100 mM MES buffer, pH 5.6, containing 4 mM EDTA to remove all of the Fe^{3+}, after which the A_{280} of this solution was read. (Note that apo-N-lobe placed into HEPES or MES buffer has an identical A_{280}.) Therefore the difference between these two readings can be assigned to the contribution of Fe^{3+} to the absorbance at 280 nm. The experimentally derived values from the Edelhoch method were used to measure the concentration of each mutant because they provide the most accurate determinations. The results of using the theoretical calculation (*32*) and the values obtained from the Edelhoch method (*31*) that uses experimental data are presented in Table 2. While in some instances the calculated and experimental values are similar (for example, within 3.3% for WT N-lobe), the value for the mutant containing only Trp264 differs by 11.4%. Additionally, the presence of Fe^{3+} results in an average increase of ~24% in the ϵ_{280} compared to the apo conformation.

Kinetics of Fe^{3+} Release. Fe^{3+} release from the WT N-lobe, double, and null tryptophan mutants was monitored at pH 5.6 at 25 °C on an Applied Photophysics SX1.8MV stopped-flow spectrofluorometer fitted with a 20 μL observation cell with a 2 nm light path and a dead time of ~1.1 ms. One syringe contained protein (375 nM) in Milli-Q water and the other syringe contained MES buffer (200 mM, pH 5.6) and EDTA (8 mM). The samples were excited at 280 nm (wavelength selection from a monochromator) and fluorescence emission was monitored by use of a high-pass 320 nm cut-on filter. For measuring the change in absorbance at 470 nm, we used the absorbance detector on the same stopped-flow instrument. For these experiments, one syringe contained protein (7.5 μM) in Milli-Q water and the other syringe contained MES buffer (200 mM, pH 5.6) and EDTA (8 mM). Rate constants were determined by fitting the change in absorbance or fluorescence intensity versus time by use of Origin software (version 7.5).

Steady-State Fluorescence Spectroscopy. Steady-state tryptophan fluorescence spectra were obtained on a Quantamaster-6 spectrofluorometer (Photon Technology International, South Brunswick, NJ) equipped with a 75-W xenon arc lamp excitation source, excitation/emission monochromators, and a WG-320 nm cut-on emission filter. Samples were excited at 280 or 295 nm and emission scans were collected from 295 to 400 nm or from 305 to 400 nm, respectively, with slit widths of 1 nm (excitation) and 4 nm (emission). All spectra were corrected for Raman scattering and background fluorescence by subtraction of the appropriate buffer blank. To allow us to directly compare the intensity between each mutant, fluorescence scans were collected on the same day on the same instrument. Fe^{3+}-containing protein (1 μM) was added to a cuvette (1.8 mL final volume) containing 100 mM HEPES buffer, pH 7.4, at 25 °C and gently stirred with a small magnetic stir bar. Apo-protein was obtained by adding the same amount of iron protein to 100 mM MES, pH 5.6, with 4 mM EDTA and allowing the mixture to equilibrate for ~20 min. Three steady-state emission scans were collected and averaged.

Free Cysteine Determination by Use of Ellman's Reagent (DTNB). Determination of the number of free cysteine residues in the N-lobe and the Trp8 mutant after UV excitation was by a standard spectrophotometric assay (*33*). Briefly, the double mutant containing only Trp8 (17.3 μM) in 2 mL of 100 mM HEPES, pH 7.4, was irradiated with 295 nm light, under steady-state conditions, for varying amounts of time between 10 and 60 min. The slits on the

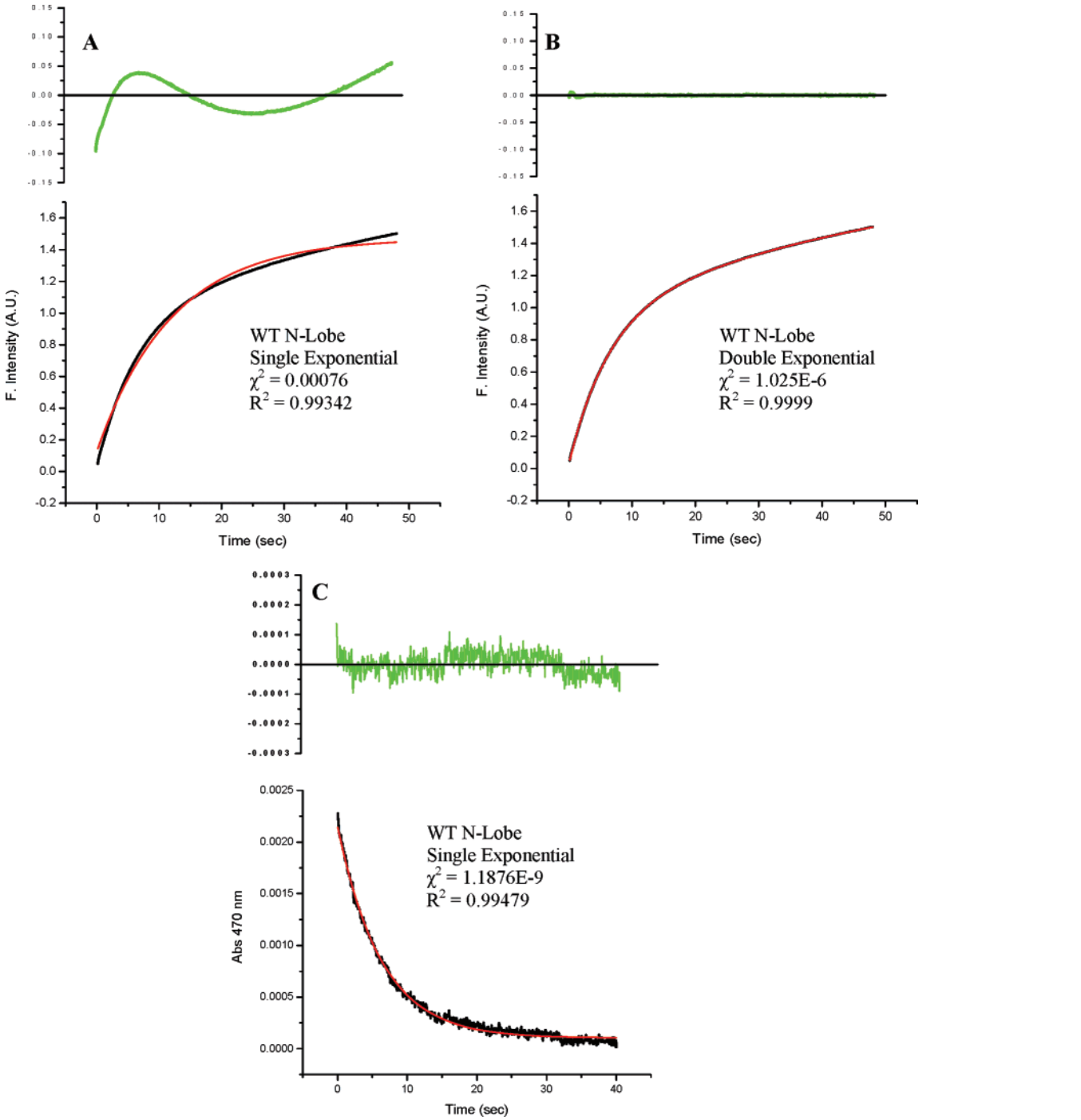

FIGURE 2: Iron release curve for WT N-lobe at pH 5.6. Fe^{3+}-bound sample (375 nM) was rapidly mixed with MES buffer, pH 5.6, containing EDTA and excited at 280 nm. The fluorescence emission was monitored by use of a 320 nm cut-on filter. Single- (A) and double-exponential fits (B) are shown. The residuals (green) clearly demonstrate that the choice of the double-exponential fit is justified. The double-exponential fit of the fluorescence data for the WT N-lobe gives rates of 8.9 ± 0.8 min^{-1} and 1.3 ± 0.3 min^{-1} (Table 2). (C) Loss of iron, directly monitored by measuring loss of signal at the visible absorption maximum of 470 nm. The single-exponential fit of the visible absorbance data gives a value of 9.1 ± 0.7 min^{-1}, n = 20, and allows assignment of the first rate in the fit of the fluorescence data in panel B directly to iron release.

excitation monochromator were opened to 2 nm to increase the amount of excitation light. Excess DTNB (100 μL of an 8.5 mM stock solution in methanol) was added to 900 μL of the Trp8 mutant after exposure to the UV radiation. The absorbance was recorded after ~20 min of incubation with DTNB. An identical sample, not subjected to UV irradiation, served as the blank. The increase in absorbance at 412 nm was monitored and corresponds to the release of the nitrothiobenzoate ion (ϵ_{412nm} = 13 600 M^{-1} cm^{-1}); the number of free cysteine residues is proportional to this value (*33*).

RESULTS

Fe^{3+} Release from WT N-Lobe. Fe^{3+} release from the WT N-lobe at the physiologically relevant pH of 5.6 yielded a hyperbolic curve that clearly fits to a double-exponential function better than to a single-exponential function (Figure 2A,B). The double-exponential fit of the fluorescence data

Table 1: Iron Release Rate Constants[a]

protein	k_{obsN1} (min^{-1})	k_1 (*x*-fold difference vs WT)	k_{obsN2} (min^{-1})	k_2 (*x*-fold difference vs WT)	I_1/I_2[b] (%)
WT N-lobe	8.9 ± 0.8	1	1.3 ± 0.3	1	64/36
Trp8	19.6 ± 0.7	2	1.1 ± 0.1	1	26/74
Trp128	37.5 ± 2.3	4	3.7 ± 0.3	3	58/42
Trp264	44.6 ± 3.6	5	4.7 ± 0.3	4	60/40
null Trp	low signal				

[a] At pH 5.6, in 100 mM MES buffer containing 4 mM EDTA as chelator and protein concentration of 375 nM. Iron release was monitored by fluorescence as described under Materials and Methods. Each value represents an average of 3−6 runs. [b] I_1 and I_2 refer to the changes in intensity corresponding to k_{obsN1} and k_{obsN2}, respectively.

for the WT N-lobe yielded rate constants of 8.9 ± 0.8 min^{-1} and 1.3 ± 0.3 min^{-1}. In an effort to provide a physical basis for these two rate constants, we measured the release of iron *directly* by monitoring the loss of signal at 470 nm (the visible absorption maximum for iron binding) at pH 5.6 (Figure 2C). This experiment is technically challenging because the visible signal is low relative to the UV signal at 280 nm (ratio of ∼1:20) and especially relative to the fluorescent signal. Given the small change in absorbance, the experiment was repeated with three different preparations of WT N-lobe on different days to be certain that the results are reproducible. Significantly, the visible absorbance data fit well to a single-exponential function (Figure 2C) and yielded a value of 9.1 ± 0.7 min^{-1}, allowing assignment of the faster rate constant in the fit of the fluorescence data directly to iron release. In an effort to understand the structural basis of the complex fluorescent transient upon iron release and in particular the slower event that follows it, we produced mutants in which a single Trp residue remained in each of the positions (8, 128, and 264) or in which all three Trp residues were eliminated (null Trp mutant). The constructs were expressed by BHK cells and secreted into the tissue culture medium. WT N-lobe expression generally exceeds 50 mg/L (*30*). The three double mutants were produced in a range of 19−35 mg/L, whereas the null Trp mutant reached a maximum of only ∼8 mg/L.

Fe^{3+} Release from Mutants. Data were collected for each of the mutants at the putative endosomal pH of 5.6 (Table 1). Curves for the pH 5.6 data for the WT and mutant proteins are presented in Figure 3. In each case, a double-exponential function clearly gives a better fit than a single-exponential function (see Figure 2A and B for the WT protein and Supporting Information Figure 2 for the mutants). Significantly, at pH 5.6, we were unable to measure a rate constant(s) for the null Trp mutant (Figure 3 and Table 1). Additionally, the double mutant containing only Trp8 had a lower signal than the other two double point Trp mutants (Figure 3).

Absorbance Spectra. Iron-saturated hTF has a characteristic spectral signature centered at ∼470 nm, giving rise to a pink color. This results from the ligand to metal charge transfer between Fe^{3+} and the two tyrosine ligands (*18*). Since iron coordination also contributes to the UV spectrum, both λ_{max} and A_{280}/A_{max} are determined for each new mutant to allow comparisons of the effect on the iron coordination from a mutation. (Note that A_{max} refers to the absorbance at λ_{max}). In comparison to the WT N-lobe, the mutant containing

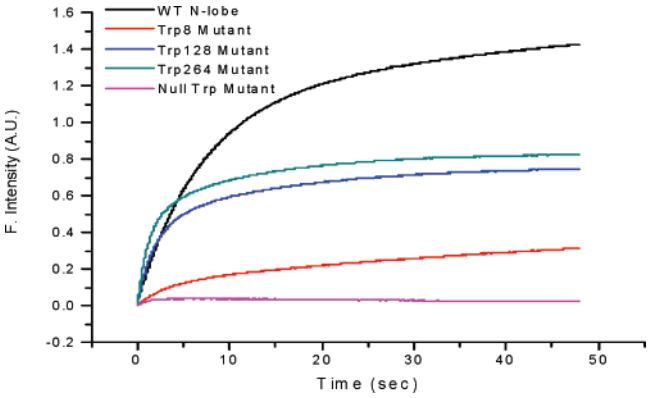

FIGURE 3: Iron release curves for WT N-lobe, the three double mutants, and null Trp mutant at pH 5.6. Each curve represents an average of at least 5 runs. Fe^{3+}-bound samples (375 nM) were rapidly mixed with MES buffer, pH 5.6, containing EDTA and excited at 280 nm. The fluorescence emission was monitored by use of a 320 nm cut-on filter. Fits for the WT N-lobe are shown in Figure 2. (Data for the mutants with single- and double-exponential fits are presented in Supporting Information Figure 2.)

only Trp8 has a λ_{max} that is 4 nm red-shifted, the mutant containing only Trp128 shows a 2 nm blue shift, and the mutant containing only Trp264 shows no change in λ_{max} (Table 2). The WT N-lobe has an A_{280}/A_{max} ratio of 23.5. The Trp8 and null Trp mutants have similar ratios to the WT protein, whereas the mutants containing only Trp128 and Trp264 have lower A_{280}/A_{max} ratios. This observation means that A_{280} is lower and/or A_{max} is higher. The results show that the contributions of each of the Trp residues to the absorbance spectrum are not the same.

Steady-State Fluorescence Spectra. The fluorescence spectra of the three double mutants and of the null Trp mutant were determined in the presence or absence of Fe^{3+} at an excitation wavelength of 295 nm. The results, relative intensity (compared in counts per second), and λ_{max} are presented in Table 3. In transitioning from the Fe^{3+}-bound to the apo form, the fluorescent signal for the WT N-lobe increases 216%, and the double mutants containing only Trp8, Trp128, and Trp264 increase 12%, 127%, and 63%, respectively. Comparison of the Fe^{3+} form and the apo form shows that the WT N-lobe undergoes a 4 nm spectral blue shift, the Trp128 mutant is shifted by 3 nm and the Trp8 and Trp264 mutants remain unchanged. Except for the Trp8 and the null Trp mutants, nearly identical results were obtained when samples were excited at 280 nm (Supporting Information Table 1). (These data are included to allow direct comparison to the Fe^{3+} release data, in which excitation was at 280 nm.)

Steady-state fluorescence spectra of the null Trp mutant with and without Fe^{3+} are similar (Table 3); additionally, the molecular mass of the mutant is consistent with the conversion of the three Trp residues to tyrosines (Table 1). This mutant serves as an important control that allows us to assign the change in the fluorescence signal entirely to the Trp residues (without any significant contribution from the tyrosine residues). To more completely evaluate the null Trp mutant, a fluorescence spectrum of the sample in the presence of 6 M GdnHCl was collected. As shown in Supporting Information Figure 3, a peak at 307 nm is observed, as well as a shoulder centered at ∼350 nm. Acidification causes the

Table 2: Summary of Spectral Characteristics and Absorption for the WT N-Lobe and Tryptophan Mutants

N-lobe	λ_{max} (nm)	A_{280}/A_{max}	M_r calcd	M_r exptl[a]	ϵ_{280} apo (mM) calcd[b]	ϵ_{280} apo (mM) exptl[c]	ϵ_{280} iron[d] (mM)
WT	472	23.5	37 151	37 151 ± 1	38.4	40.3 ± 0.2	50.7 ± 0.4
Trp8	476	24.3	37 106	37 106 ± 1	30.3	32.6 ± 0.8	38.9 ± 0.5
Trp128	470	16.1	37 106	37 109 ± 1	30.3	31.5 ± 1.0	38.7 ± 1.0
Trp264	472	19.2	37 106	37 109 ± 1	30.3	34.2 ± 0.8	42.4 ± 0.7
null Trp	468	22.2	37 082	37 084 ± 1	26.3	28.4 ± 0.3	35.5 ± 0.5

[a] Electrospray ionization mass spectra were obtained on a JMS-700 MStation (JEOL, Tokyo, Japan) two-sector mass spectrometer equipped with a standard ESI source (*41*). [b] Absorption coefficients were calculated as described (*32*). [c] Determined as described by Edelhoch (*31*). [d] We experimentally determined the contribution of iron to the absorbance at 280 nm and corrected for it to derive ϵ_{280} for the iron form as described under Materials and Methods.

Table 3: Fluorescence Properties WT N-Lobe of hTF and Various Mutants Excited at 295 nm

hTF N-lobe[a]	rel fluorescence intensity at λ_{max}	λ_{max} (nm)
WT (apo)	192 000	338
WT (iron)	60 800	342
Trp8 (apo)	36 900[b]	342
Trp8 (iron)	33 100[c]	342
Trp128 (apo)	108 000	338
Trp128 (iron)	47 500	341
Trp264 (apo)	147 000	342
Trp264 (iron)	90 300	342
null Trp (apo)	72 000	342
null Trp (iron)	73 000	344

[a] Samples contained 1 μM protein. Scans of the iron-containing samples were in HEPES buffer and those of the apo samples were in MES buffer as described under Materials and Methods. [b] Value was 43 000 at 60 min. [c] Value was 39 000 at 10 min.

shoulder to decrease considerably, indicating that one (or more) of the 17 tyrosine residues in this mutant is ionized and exists as a tyrosinate ion(s) (see Discussion).

Detection of Cystine Reduction upon Extended Excitation of Trp8. Although there is a relatively small increase in the fluorescent signal when Fe^{3+} is removed from the mutant containing Trp8, we noted a time-dependent fluorescence increase upon excitation at 295 nm (Figure 4 and Table 3). The increase reaches a plateau at 60 min for the apo protein and 10 min for the Fe^{3+} form. Further excitation leads to a decrease in the signal attributed to photobleaching (not shown). Since the 16 cysteine residues in the N-lobe are engaged in disulfide bonds, titration of the WT N-lobe with DTNB showed no free cysteine as would be expected. However, it is quite common for disulfide bonds to reside close to tryptophan and/or other aromatic residues. In fact, it has been suggested that these residues may help to stabilize correct folding of a protein (*33*, *34*). A number of studies have also shown that excited-state energy from Trp residues can induce disulfide bond reduction, which is detected as an increase in the fluorescence intensity over time (when constantly exposed to 295 nm light) (*33*, *35*). Given the steady-state fluorescence data and the location of Trp8 (Figure 1), photoreduction of nearby disulfide bonds provides a plausible explanation for the increase in fluorescence intensity that is observed over time. Additionally, upon constant excitation with 295 nm light, the Trp8 mutant showed an increase in the concentration of free thiol on the same time scale as the enhancement of its fluorescence signal. At the plateau, ~4 free thiol groups are liberated, consistent with two nearby disulfides (data not shown).

DISCUSSION

To our surprise, iron release from the WT N-lobe at pH 5.6 on a new, more sensitive, Applied Photophysics stopped-flow spectrofluorometer resulted in a curve for which a double-exponential function clearly provides a better fit than a single-exponential function (see Figure 2A,B). Rate constants of 8.9 ± 0.8 min^{-1} and 1.3 ± 0.3 min^{-1} were determined, accounting for 64% and 36% of the intensity change, respectively. In previous kinetic studies in which Fe^{3+} release from the N-lobe of hTF was measured at pH 5.6, only a single rate constant of 9.5 ± 0.8 min^{-1} was found, clearly matching the faster rate constant from the new data (*25*). Significantly, in the present work we were able to measure the release of Fe^{3+} *directly* by monitoring the loss of signal at the visible absorption maximum of 470 nm at pH 5.6 (Figure 2C). A value of 9.1 ± 0.7 min^{-1} was obtained, allowing assignment of the faster rate constant in the fit of the fluorescence data directly to release of Fe^{3+}.

What then is the source of the second rate constant that accounts for ~40% of the increase in the fluorescent signal from the WT N-lobe? It seems clear that it is reporting the conformational change which can only occur after Fe^{3+} is released. Without the Fe^{3+} binding to ligands and holding the cleft closed, the N-lobe is free to undergo rigid-body movement of the two subdomains leading to the full opening of the cleft. The fact that the Trp128 and Trp264 residues residing on opposite sides of the cleft (Figure 1) are reporting this change (Table 1) is consistent with a global movement that is reported locally. As detailed below, each of the three individual Trp residues resides in a unique environment, resulting in distinctive spectral properties and contributions to the fluorescent change.

There are at least four possible models that must be considered to describe the two processes obtained from the kinetic studies. Each of the four models is presented and a mathematical description justifying our chosen model is provided in an appendix in the Supporting Information. Biphasic kinetics have also been reported for iron release from the N-lobe of ovotransferrin, which, like hTF, has a dilysine "trigger" (*21*). In ovotransferrin the two rate constants are attributed to iron release from two different anion-induced conformations following two different pathways to Fe^{3+} release. In our studies, we clearly observe a single pathway with two steps: (1) Fe^{3+} release followed by (2) conformational changes resulting in cleft opening. We have no indication of possible other conformational states prior to Fe^{3+} release since a single rate constant is observed

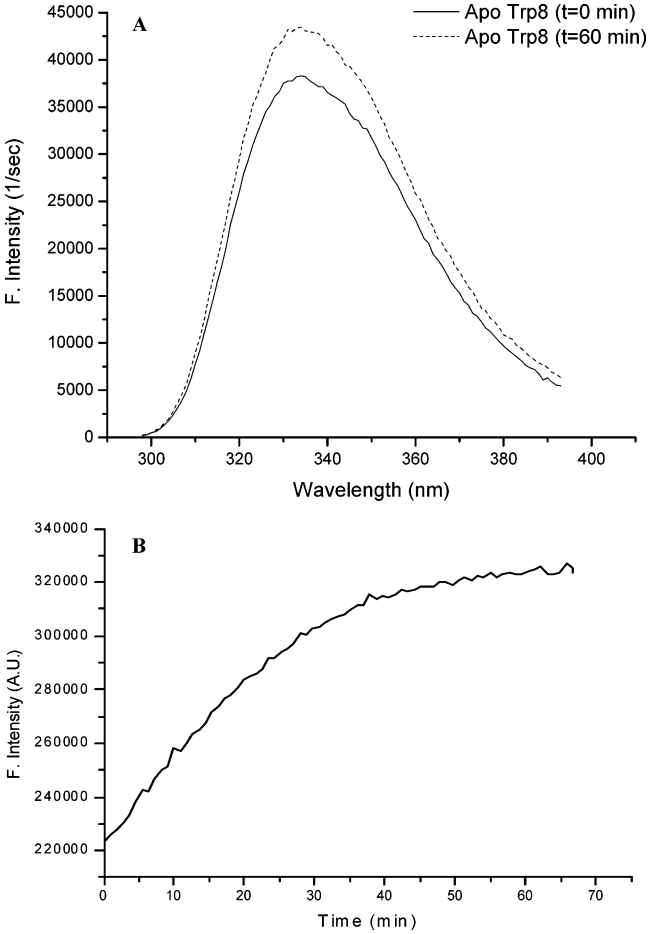

FIGURE 4: (A) Steady-state emission spectra of the double mutant containing only Trp8 at 0 and 60 min after constant excitation with 280 nm light and (B) time-based emission of the increase in fluorescence intensity at 342 nm. Excitation slits were increased from 1 (steady-state setting) to 2 nm for the time based scan.

when the disappearance of the visible absorbance at 470 nm is monitored (Figure 2C).

To more precisely determine the structural basis of the fluorescent changes, mutants in which a single Trp residue remained or which lacked all three Trp residues were produced. Although the mutants containing a single Trp residue show an increase in Fe^{3+} release relative to WT N-lobe (2−5-fold faster at pH 5.6), the rate constants indicate that mutations of the three tryptophan residues had only modest effects on the stability of the N-lobe. Importantly, the kinetic data for the Trp mutants demonstrate that the overall structure of the N-lobe is minimally compromised such that the individual Trp residues in our mutants would be expected to have photophysical properties similar to those in the WT N-lobe.

Trp8 is located in the NI subdomain in a hydrophobic box composed of three phenylalanine residues (Figure 1) (*7*, *8*). Upon excitation, Trp8 contributes very little to the fluorescent signal in either the apo or Fe^{3+} form (Table 3), probably due to excited-state electron transfer to the nearby disulfide bonds (*36*). The low signal associated with Fe^{3+} release at pH 5.6 from the mutant retaining only Trp8 (Figure 3) is completely consistent with the fact that it contributes so little to the change in the fluorescent signal. What was not predicted (or observed previously) is that extended excitation at 295 nm leads to reduction of the nearby disulfide bonds as demonstrated by the increase in fluorescence intensity (Table 3 and Figure 4). This suggestion is confirmed by titration of the Trp8 mutant with DTNB and the finding that four free thiol groups are generated. The most likely candidates for reduction are two disulfide bonds (Cys9/Cys48 and Cys19/Cys39), each within ∼7 Å of Trp8 (Figure 1). The plateau in fluorescence intensity, which is proportional to this disulfide reduction, is reached within 60 min for the apo form (Figure 4) and 10 min for the Fe^{3+} form of the mutant (data not shown). We suggest that this difference may be due to an increase in rigidity of the Fe^{3+} complex. The interaction between Trp8 and these two disulfide bonds also undoubtedly contributes to the overall stability of this region. Absence of Trp8 (as in the Trp128 and Trp264 mutants) resulted in faster rates of iron release at both pH 7.4 (data not shown) and 5.6 (Table 1) by destabilizing the local environment.

Trp128 is located in the NII subdomain, immediately preceding α-helix 5 (residues 129−135), which contains residues that bind to and stabilize the synergistic carbonate anion (including Thr120, Arg124, Ala126, and Gly127). Trp128 makes a significant contribution to the characteristic visible absorption signal (Table 2), due to both its proximity to the metal site (∼13 Å) and overlap with the Fe^{3+}−tyrosine charge-transfer band. Upon excitation at 295 nm, the fluorescent signal of this mutant increases 127% in transitioning from the Fe^{3+} to apo form and shows a 3 nm blue shift. Blue shifts have been attributed to a Trp residue becoming less solvent-exposed (more buried) and/or to changes in the orientation of the Trp ring relative to water dipoles (*37*). The structural rearrangements in the local environment of Trp128 are observed in the kinetic studies at pH 5.6 and give rise to the second slower rate constant (Table 1).

Trp264 is a surface residue located on α-helix 9 (composed of residues 260−273) in the NI subdomain (*7*, *8*). Although Trp264 is 23 Å from Fe^{3+}, its peak fluorescence emission shows a 63% increase when the double mutant containing only Trp264 loses Fe^{3+} (Table 3). Calculations from Lehrer (*22*) show that the critical transfer of excited-state energy from tryptophan to the metal center is ∼20 Å. If the distance between a tryptophan residue and Fe^{3+} is equal to (or greater than) this distance, a decrease in fluorescence intensity by other kinds of quenching is equally probable. Therefore, it seems likely that the observed difference in fluorescence intensity cannot be completely attributed to quenching by Fe^{3+} and that structural rearrangements around Trp264 occur. In the absence of a spectral shift (in absorbance or fluorescence) between the apo or iron form of this mutant, the decrease in intensity cannot be attributed to an increase in solvent exposure. Side chains of charged amino acids can facilitate electron transfer to the peptide backbone (*38*). We suggest that one or more of three nearby glutamic acid residues (Glu260 ∼12 Å, Glu265 ∼8 Å, and Glu272 ∼10 Å away from Trp264) and/or Asp261 (located ∼10 Å away) may be acting on Trp264 (Figure 1). As for the Trp128 mutant, two events are observed in our pH 5.6 kinetic assay yielding two rate constants (Table 1), assigned to removal of the iron by EDTA and the movement of Trp264 away from the nearby negatively charged residues induced by cleft opening as a result of Fe^{3+} loss.

The null Trp N-lobe mutant is an important control that allows a direct determination of the contribution of the tyrosine residues (14 in the WT N-lobe and 17 in this mutant) to the absorbance and fluorescence emission spectra. The 4 nm blue shift in the absorbance maximum of this mutant compared to the WT N-lobe reflects the missing contribution of the Trp residues and/or possible energy transfer from the tyrosine substitution for tryptophan at position 128 to the metal center. We attribute the increase in the fluorescence intensity of the null Trp mutant compared to the mutant containing only Trp8 to the quenching of Trp8 by the nearby disulfides and the added contribution of the substituted tyrosine to the signal. The absence of the three Trp residues allows observation of fluorescence from one or more putative ionized tyrosine (tyrosinate) residue(s). Proof that the source of the signal is tyrosinate comes from the significant reduction of the signal at ~350 nm upon acidification (Supporting Information Figure 3). In comparison to L-tyrosine, both the excitation and emission signals of tyrosinates are red-shifted (*39*). Additionally, UV resonance Raman spectroscopy revealed that full-length hTF contained one (or more) tyrosine residues with an unusually low pK_a of 7.57 (*40*). Confirmation of this observation with the isolated N-lobe is of interest when the crucial role that tyrosine residues (Tyr95 and Tyr188) play in iron binding is considered. Efforts to measure iron release from the triple-null Trp mutant give a very weak signal, as predicted from the small difference (14%) in the fluorescent signal in the apo and iron forms compared to the other constructs (Table 3).

In summary, Trp128 and Trp264 almost completely account for the change in fluorescence monitored by Fe^{3+} release assays from the N-lobe. At pH 5.6, two fluorescent changes are reported, reflecting loss of quenching due to iron removal and structural rearrangements in the local environments of these Trp residues that contribute to a readout of the more global change in which the cleft opens. Trp8 interacts with and stabilizes two disulfide bonds (and is quenched by them). The null Trp mutant demonstrates the importance of the tryptophan residues in the characteristic absorbance peak and the almost complete lack of any contribution of tyrosine residues in the assay monitored by fluorescence. The presence of one or more tyrosinate residues is also documented in this mutant. Further studies will be required to determine whether the presence of the C-lobe changes the kinetic parameters reported here for the isolated N-lobe.

ACKNOWLEDGMENT

We are very grateful to Dr. Igor Kaltashov and to Mingxuan Zhang for providing the electrospray ionization mass spectra of the double and triple null Trp mutants. We thank Dr. Iwona Buskiewicz for technical assistance in use of the Applied Photophysics SX1.8MV stopped-flow spectrofluorometer. We are grateful to the Dean's Office at the University of Vermont, College of Medicine for purchase of this instrument.

SUPPORTING INFORMATION AVAILABLE

Table showing fluorescent properties upon excitation at 280 nm; figures showing iron release from WT N-lobe at pH 5.6 on Olis-RSM 1000 spectrofluorometer, single- vs double-exponential fits for iron release from Trp8, Trp128, and Trp264, and fluorescent steady-state scans of null Trp mutant in bicarbonate and 6 M GdnHCl; and an appendix in which four models for biphasic kinetics are presented and a single final model is mathematically justified. This material is available free of charge via the Internet at http://pubs.acs.org.

REFERENCES

1. Aisen, P., Enns, C., and Wessling-Resnick, M. (2001) Chemistry and biology of eukaryotic iron metabolism, *Int. J. Biochem. Cell Biol. 33*, 940−959.
2. He, Q.-Y., and Mason, A. B. (2002) Molecular aspects of release of iron from transferrins, in *Molecular and Cellular Iron Transport* (Templeton, D. M., Ed.) pp 95−123, Marcel Dekker, Inc, New York.
3. Klausner, R. D., van Renswoude, J., Ashwell, G., Kempf, C., Schechter, A. N., Dean, A., and Bridges, K. R. (1983) Receptor-mediated endocytosis of transferrin in K562 cells, *J. Biol. Chem. 258*, 4715−4724.
4. Klausner, R. D., Ashwell, G., van Renswoude, J., Harford, J. B., and Bridges, K. R. (1983) Binding of apotransferrin to K562 cells: explanation of the transferrin cycle, *Proc. Natl. Acad. Sci. U.S.A. 80*, 2263−2266.
5. Anderson, B. F., Baker, H. M., Norris, G. E., Rice, D. W., and Baker, E. N. (1989) Structure of human lactoferrin: Crystallographic structure analysis and refinement at 2.8 Å resolution, *J. Mol. Biol. 209*, 711−734.
6. Lambert, L. A., Perri, H., Halbrooks, P. J., and Mason, A. B. (2005) Evolution of the transferrin family: Conservation of residues associated with iron and anion binding, *Comp. Biochem. Physiol. B 142*, 129−141.
7. Jeffrey, P. D., Bewley, M. C., MacGillivray, R. T. A., Mason, A. B., Woodworth, R. C., and Baker, E. N. (1998) Ligand-induced conformational change in transferrins: crystal structure of the open form of the N-terminal half-molecule of human transferrin, *Biochemistry 37*, 13978−13986.
8. MacGillivray, R. T. A., Moore, S. A., Chen, J., Anderson, B. F., Baker, H., Luo, Y. G., Bewley, M., Smith, C. A., Murphy, M. E., Wang, Y., Mason, A. B., Woodworth, R. C., Brayer, G. D., and Baker, E. N. (1998) Two high-resolution crystal structures of the recombinant N-lobe of human transferrin reveal a structural change implicated in iron release, *Biochemistry 37*, 7919−7928.
9. Wally, J., Halbrooks, P. J., Vonrhein, C., Rould, M. A., Everse, S. J., Mason, A. B., and Buchanan, S. K. (2006) The crystal structure of iron-free human serum transferrin provides insight into inter-lobe communication and receptor binding, *J. Biol. Chem. 281*, 24934−24944.
10. Dewan, J. C., Mikami, B., Hirose, M., and Sacchettini, J. C. (1993) Structural evidence for a pH-sensitive dilysine trigger in the hen ovotransferrin N-lobe: Implications for transferrin iron release, *Biochemistry 32*, 11963−11968.
11. He, Q.-Y., Mason, A. B., Tam, B. M., MacGillivray, R. T. A., and Woodworth, R. C. (1999) Dual role of Lys206−Lys296 interaction in human transferrin N-lobe: Iron-release trigger and anion-binding site, *Biochemistry 38*, 9704−9711.
12. Harris, D. C., and Aisen, P. (1989) Physical Biochemistry of the Transferrins, in *Iron Carriers and Iron Proteins* (Loehr, T. M., Ed.) pp 239−351, VCH Publishing, Inc., New York.
13. Lin, L.-N., Mason, A. B., Woodworth, R. C., and Brandts, J. F. (1994) Calorimetric Studies of Serum Transferrin and Ovotransferrin. Estimates of Domain Interactions, and Study of the Kinetic Complexities of Ferric Ion Binding, *Biochemistry 33*, 1881−1888.
14. Halbrooks, P. J., He, Q. Y., Briggs, S. K., Everse, S. J., Smith, V. C., MacGillivray, R. T. A., and Mason, A. B. (2003) Investigation of the Mechanism of Iron Release from the C-Lobe of Human Serum Transferrin: Mutational Analysis of the Role of a pH Sensitive Triad, *Biochemistry 42*, 3701−3707.
15. He, Q.-Y., Mason, A. B., Woodworth, R. C., Tam, B. M., Wadsworth, T., and MacGillivray, R. T. A. (1997) Effects of mutations of aspartic acid 63 on the metal-binding properties of the recombinant N-lobe of human serum transferrin, *Biochemistry 36*, 5522−5528.

16. He, Q.-Y., Mason, A. B., and Woodworth, R. C. (1997) Iron release from recombinant N-lobe and single point Asp 63 mutants of human transferrin by EDTA, *Biochem. J. 328*, 439−445.
17. Mason, A. B., He, Q.-Y., Tam, B. M., MacGillivray, R. T. A., and Woodworth, R. C. (1998) Mutagenesis of the aspartic acid ligands in human serum transferrin: lobe-lobe interaction and conformation as revealed by antibody, receptor-binding and iron-release studies, *Biochem. J. 330*, 35−40.
18. Patch, M. G., and Carrano, C. J. (1981) The origin of the visible absorption in metal transferrins, *Inorg. Chim. Acta 56*, L71−L73.
19. Bali, P. K., and Harris, W. R. (1989) Cooperativity and Heterogeneity between the Two Binding Sites of Diferric Transferrin during Iron Removal by Pyrophosphate, *J. Am. Chem. Soc. 111*, 4457−4461.
20. Foley, A. A., and Bates, G. W. (1988) The influence of inorganic anions on the formation and the stability of Fe(3+)-transferrin-anion complexes, *Biochim. Biophys. Acta 965*, 154−162.
21. Muralidhara, B. K., and Hirose, M. (2000) Anion-mediated iron release from transferrins─The kinetic and mechanistic model for N-lobe of ovotransferrin, *J. Biol. Chem. 275*, 12463−12469.
22. Lehrer, S. S. (1969) Fluorescence and absorption studies of the binding of copper and iron to transferrin, *J. Biol. Chem. 244*, 3613−3617.
23. Evans, R. W., and Holbrook, J. J. (1975) Differences in the protein fluorescence of the two iron(III)-binding sites of ovotransferrin, *Biochem. J. 145*, 201−207.
24. He, Q. Y., Mason, A. B., Lyons, B. A., Tam, B. M., Nguyen, V., MacGillivray, R. T. A., and Woodworth, R. C. (2001) Spectral and metal-binding properties of three single-point tryptophan mutants of the human transferrin N-lobe, *Biochem. J. 354*, 423−429.
25. Mason, A. B., Halbrooks, P. J., James, N. G., Connolly, S. A., Larouche, J. R., Smith, V. C., MacGillivray, R. T. A., and Chasteen, N. D. (2005) Mutational analysis of C-lobe ligands of human serum transferrin: insights into the mechanism of iron release, *Biochemistry 44*, 8013−8021.
26. Zak, O., Aisen, P., Crawley, J. B., Joannou, C. L., Patel, K. J., Rafiq, M., and Evans, R. W. (1995) Iron release from recombinant N-lobe and mutants of human transferrin, *Biochemistry 34*, 14428−14434.
27. Callis, P. R. (1997) 1La and 1Lb transitions of tryptophan: applications of theory and experimental observations to fluorescence of proteins, *Methods Enzymol. 278*, 113−150.
28. Yengo, C. M., Chrin, L., Rovner, A. S., and Berger, C. L. (1999) Intrinsic tryptophan fluorescence identifies specific conformational changes at the actomyosin interface upon actin binding and ADP release, *Biochemistry 38*, 14515−14523.
29. Funk, W. D., MacGillivray, R. T. A., Mason, A. B., Brown, S. A., and Woodworth, R. C. (1990) Expression of the amino-terminal half-molecule of human serum transferrin in cultured cells and characterization of the recombinant protein, *Biochemistry 29*, 1654−1660.
30. Mason, A. B., Funk, W. D., MacGillivray, R. T. A., and Woodworth, R. C. (1991) Efficient production and isolation of recombinant amino-terminal half-molecule of human serum transferrin from baby hamster kidney cells, *Protein Expression Purif. 2*, 214−220.
31. Edelhoch, H. (1967) Spectroscopic Determination of Tryptophan and Tyrosine in Proteins, *Biochemistry 6*, 1948−1954.
32. Pace, C. N., Vajdos, F., Fee, L., Grimsley, G., and Gray, T. (1995) How to measure and predict the molar absorption coefficient of a protein, *Protein Sci. 4*, 2411−2423.
33. Neves-Petersen, M. T., Gryczynski, Z., Lakowicz, J., Fojan, P., Pedersen, S., Petersen, E., and Bjorn, P. S. (2002) High probability of disrupting a disulphide bridge mediated by an endogenous excited tryptophan residue, *Protein Sci. 11*, 588−600.
34. Petersen, M. T. N., Jonson, P. H., and Petersen, S. B. (1999) Amino acid neighbours and detailed conformational analysis of cysteines in proteins, *Protein Eng. 12*, 535−548.
35. Prompers, J. J., Hilbers, C. W., and Pepermans, H. A. (1999) Tryptophan mediated photoreduction of disulfide bond causes unusual fluorescence behaviour of *Fusarium solani pisi* cutinase, *FEBS Lett. 456*, 409−416.
36. Chen, Y., and Barkley, M. D. (1998) Toward understanding tryptophan fluorescence in proteins, *Biochemistry 37*, 9976−9982.
37. Vivian, J. T., and Callis, P. R. (2001) Mechanisms of tryptophan fluorescence shifts in proteins, *Biophys. J. 80*, 2093−2109.
38. Callis, P. R., and Liu, T. (2004) Quantitative prediction of fluorescence quantum yields for tryptophan in proteins, *J. Phys. Chem. B 108*, 4248−4259.
39. Lakowicz, J. R. (2006) *Principles of Fluorescence Spectroscopy*, 3rd ed., Springer, New York.
40. Clarkson, J., and Smith, D. A. (2001) UV Raman evidence of a tyrosine in apo-human serum transferrin with a low pK_a that is elevated upon binding of sulphate, *FEBS Lett. 503*, 30−34.
41. Byrne, S. L., Leverence, R., Klein, J. S., Giannetti, A. M., Smith, V. C., MacGillivray, R. T. A., Kaltashov, I. A., and Mason, A. B. (2006) Effect of glycosylation on the function of a soluble, recombinant form of the transferrin receptor, *Biochemistry 45*, 6663−6673.

BI602425C